



Production rate calibration for cosmogenic ^{10}Be in pyroxene by applying a rapid fusion method to ^{10}Be -saturated samples from the Transantarctic Mountains, Antarctica.

Marie Bergelin¹, Greg Balco^{2,1}, Lee B. Corbett³ and Paul R. Bierman³

5 ¹Berkeley Geochronology Center, Berkeley, CA

²Lawrence Livermore National Lab, Livermore, CA

³Rubenstein School of the Environment and Natural Resources, University of Vermont/National Science Foundation Community Cosmogenic Facility.

Correspondence to: Marie Bergelin (mbergelin@bgc.org)

10 **Abstract**

Measurements of multiple cosmogenic nuclides in a single sample are valuable for various applications of cosmogenic nuclide exposure dating and allow for correcting exposure ages for surface weathering and erosion and establishing exposure-burial history. Here we provide advances in the measurement of cosmogenic ^{10}Be in pyroxene and constraints on the production rate which provide new opportunities for measurements of multi-nuclide systems, such as $^{10}\text{Be}/^3\text{He}$, in
15 pyroxene-bearing samples. We extracted and measured cosmogenic ^{10}Be in pyroxene from two sets of Ferrar Dolerite samples collected from the Transantarctic Mountains in Antarctica. One set of samples has ^{10}Be concentrations close to saturation which allows for the production rate calibration of ^{10}Be in pyroxene by assuming production-erosion equilibrium. The other set of samples, which has a more recent exposure history, is used to determine if a rapid fusion method can be successfully applied to samples with Holocene to Last-Glacial-Maximum exposure ages. From measured ^{10}Be concentrations
20 in the near-saturation sample set we find the production rate of ^{10}Be in pyroxene to be 3.74 ± 0.10 atoms $\text{g}^{-1} \text{yr}^{-1}$ and is consistent with $^{10}\text{Be}/^3\text{He}$ paired nuclide ratios from samples assumed to have simple exposure. Given the high ^{10}Be concentration measured in this sample set, a sample mass of ~ 0.5 g of pyroxene is sufficient for the extraction of cosmogenic ^{10}Be from pyroxene using a rapid fusion method. However, for the set of samples having low ^{10}Be concentrations, measured concentrations were higher than expected. We attribute spuriously high ^{10}Be concentration to potential failure in removing
25 all meteoric ^{10}Be and/or a highly variable and poorly quantified measurement background.

1 Introduction

This paper describes advances in the measurement and application of cosmogenic ^{10}Be in pyroxene, including a rapid fusion extraction method and a production rate calibration data set. This is important because measurements of multiple cosmogenic nuclides in single samples are valuable for various applications of exposure dating. Multiple-nuclide systematics



30 are useful for correcting exposure ages for surface weathering and erosion (Klein et al., 1986; Nishiizumi et al., 1986; Lal, 1991), as well as quantifying when and how often a surface has experienced burial (Granger and Muzikar, 2001; Granger, 2006; Balco and Rovey, 2008). For quartz-rich samples, paired $^{26}\text{Al}/^{10}\text{Be}/^{21}\text{Ne}$ measurements in quartz are common practice and well-established (e.g. Balco and Shuster, 2009). However, multiple-nuclide measurements are generally not feasible in minerals other than quartz.

35

The stable cosmogenic nuclide ^3He is most commonly used in mafic rocks for exposure dating, as it is retentive in both pyroxene and olivine (Blard, 2021) and easily measured using a noble gas mass spectrometer (Balter-Kennedy et al., 2020). Measurements of cosmogenic ^{10}Be in pyroxene are potentially useful for exposure age applications and have been investigated in prior studies (Balter-Kennedy et al., 2020; Blard et al., 2008; Collins, 2015; Eaves et al., 2018; Ivy-Ochs et al., 1998; Nishiizumi et al., 1990). To fully utilize multiple nuclides in pyroxene, it is necessary to constrain the production rate of cosmogenic ^{10}Be in pyroxene.

Cosmogenic nuclide production rates can be quantified in samples by (i) constraining the exposure age by independent radiocarbon and/or other geological dating methods (e.g. Borchers et al., 2016; Blard et al., 2008; Eaves et al., 2018), (ii) measuring the ratio of one nuclide to another with an already well-known production rate (e.g. Niedermann et al., 1994), and/or (iii) samples experiencing negligible erosion rates and where the nuclide concentration has reached production-erosion equilibrium (Borchers et al., 2016; Jull et al., 1989; Nishiizumi et al., 1986). In this study, we take advantage of some of the longest exposed rocks in central Antarctica, where erosion rates are negligible, and ^3He exposure ages exceeding 8 Ma require that ^{10}Be concentrations must be close to the production-erosion equilibrium (Balter-Kennedy et al., 2020). This provides an opportunity to validate the previously suggested ^{10}Be production rate in pyroxene constrained by the different approaches described above.

Previously, extraction of ^{10}Be from pyroxene (e.g. Balter-Kennedy et al., 2020; Blard et al., 2008; Collins, 2015; Eaves et al., 2018) has used wet chemical dissolution and column chromatography similar to that for extracting ^{10}Be from quartz (Corbett et al., 2016). However, this process is challenging because of the large cation load and the extremely high selectivity required in the column separation. We adopt a ^{10}Be extraction method involving a total rapid fusion of the pyroxene sample (Stone, 1998) to improve the efficiency of ^{10}Be extraction from pyroxene. This method is commonly used to extract meteoric ^{10}Be from a variety of geologic matrices and should therefore be applicable for pyroxene despite the high concentrations of other cations.

60

We apply the fusion method to two sets of samples. First, we analyze a set of samples with extremely high ^{10}Be concentrations (10^7 atoms g^{-1}) that, as described above, can be used for production rate calibration by assuming production-



erosion equilibrium. Second, we analyze an additional set of samples with much lower ^{10}Be concentrations (10^4 - 10^5 atoms g^{-1}) to determine if the fusion method can be successfully applied to samples with Holocene to Last-Glacial-Maximum exposure ages.

2 Method

2.1 Geological Setting and Samples

We selected two sets of samples of Ferrar Dolerite from the Transantarctic Mountains (TAM). The Ferrar Dolerite (Harvey, 2001) is a mafic intrusive rock consisting primarily of calcic plagioclase and several ortho- and clinopyroxenes (Elliot and Fleming, 2021). The first set consists of 10 samples from the upper TAM that had previous ^3He measurements indicating exposure ages > 8 Ma. These samples are surface boulders collected from various moraines from Roberts Massif described by Balter-Kennedy et al. (2020) and several similar samples from nearby Otway Massif (Table 1). The Otway Massif data are not described in a publication but are available in the ICE-D database (www.ice-d.org) due to public release requirements of the funding agency. Erosion rates for Ferrar Dolerite in Antarctica are 0 - 35 cm Myr^{-1} (Balter-Kennedy et al., 2020). However, the ^3He exposure ages limit the erosion rates for these specific samples to be < 5 cm yr^{-1} , and therefore, this set of samples can be expected to have reached production-decay equilibrium (“saturation”) for ^{10}Be , such that $N_{10} = P_{10}/\lambda_{10}$. After 8 Ma of exposure, ^{10}Be concentrations have reached 98% of saturation values. Thus, these samples are expected to have extremely high ^{10}Be concentrations, facilitating precise measurements. Measuring ^{10}Be in these samples allows a straightforward estimate of the ^{10}Be production rate in pyroxene integrated over the last 8 Ma.

The second set of samples is designed to test whether or not the fusion extraction method is also effective for samples with lower ^{10}Be concentrations. The samples we analyze are low-elevation glacially transported erratics near outlet glaciers of the East Antarctic Ice Sheet in Northern Victoria Land. Exposure-age chronologies using ^{10}Be in quartz or ^3He in pyroxene from the same sites indicate that these samples have exposure ages of the last glacial-interglacial cycle. In addition, ^{10}Be in pyroxene was previously measured in two of these samples (MG-12 and MG-19) using a dissolution/cation exchange method by Eaves et al. (2018). We selected this set of samples in part because they had been analyzed for ^3He in previous studies (Table 1). We made several additional ^3He measurements so that the entire sample set now has both ^3He and ^{10}Be data. The ^3He data provide a means of evaluating the accuracy of the ^{10}Be measurements. Details of the previously analyzed samples are from Stutz et al. (2021) and Eaves et al. (2018) and are summarized in Table 1.



Table 1. Location and site information for samples of Ferrar Dolerite analyzed in this study.

Sample ID	Location	Latitude (Degrees)	Longitude (Degrees)	Elevation (m)	Thickness (cm)	Shielding	Prior Publication
15-ROB-07	Roberts Massif	-85.5249	-177.7249	2255	2.0	0.9939	Balter-Kennedy et al., (2020)
15-ROB-27	Roberts Massif	-85.5219	-177.7279	2247	4.8	0.9959	Balter-Kennedy et al., (2020)
15-ROB-30	Roberts Massif	-85.5101	-177.7943	2385	4.4	1.0000	Balter-Kennedy et al., (2020)
15-ROB-31	Roberts Massif	-85.5090	-177.7788	2369	4.3	1.0000	Balter-Kennedy et al., (2020)
15-OTW-50	Otway Massif	-85.4159	172.8086	2268	1.4	0.9967	Unpublished
15-OTW-55	Otway Massif	-85.4150	172.7819	2292	2.7	0.9962	Unpublished
15-OTW-56	Otway Massif	-85.4146	172.7756	2290	3.1	0.9959	Unpublished
15-OTW-57	Otway Massif	-85.4148	172.7832	2287	1.3	0.9962	Unpublished
15-OTW-58	Otway Massif	-85.4371	172.8626	2504	2.0	0.9980	Unpublished
15-OTW-60	Otway Massif	-85.4370	172.8670	2503	1.8	0.9980	Unpublished
17-HB-TC-02	Hughes Bluff	-75.3918	162.2125	120.8	1.0	0.9962	Stutz et al., (2021)
17-HB-TC-12	Hughes Bluff	-75.3957	162.2021	185.3	1.0	0.9919	Stutz et al., (2021)
17-EHW-05	Evans Heights	-75.0982	161.4989	433	1.0	1.0000	Stutz et al., (2021)
17-EHW-15	Evans Heights	-75.0947	161.4969	561	1.0	1.0000	Stutz et al., (2021)
15-MG12	MacKay Gl.	-76.9985	161.0376	1013	5.8	0.9790	Eaves et al., (2018)
15-MG19	MacKay Gl.	-76.9991	161.0406	981	4.0	0.9880	Eaves et al., (2018)

95 2.2 Mineral Separation

The samples were crushed and sieved to a grain size of 75-125 μm at which mostly monomineralic grains were observed. The samples were washed in water and then leached in 10% HCl at room temperature overnight. We then ran the sample through a magnetic separator to separate pyroxene from the less magnetic plagioclase and other minerals present.

100 At the National Science Foundation / University of Vermont Community Cosmogenic Facility (CCF), the pyroxene grains underwent HF leaching, following Balter-Kennedy et al. (2023), to remove meteoric ^{10}Be and any plagioclase attached to the pyroxene grains. A fine grain size reduces the amount of meteoric ^{10}Be stored in the grain fractures, and HF etching was found to be sufficient to remove meteoric ^{10}Be by Balter-Kennedy et al (2023), without powdering the sample as otherwise previously suggested (Blard et al., 2008). The samples were leached in HF twice; first in a solution of 1% HF in an
105 ultrasonic bath at $\sim 60^\circ\text{C}$ for 6 hours and then again in 1% HF/1% HNO_3 overnight, targeting a 20-30 % mass loss. During



HF leaching, precipitates of fluoride (MgF_2 , CaF_2) are produced and are insoluble in dilute HF. Therefore, we did a final leaching in 0.5% HNO_3 overnight in a heated ultrasonic bath to dissolve the fluoride precipitates.

2.3 Extraction and analyses of cosmogenic ^{10}Be in Pyroxene

The extraction of Be was done at the CCF by total fusion in a potassium bifluoride (KHF_2) flux according to Stone (1998).
110 Samples were processed in two separate batches; the first batch contained the high-concentration samples, and the second batch contained the low-concentration samples. The pure pyroxene samples were powdered using a shatterbox, and 0.5 g of powdered sample was massed into 30 mL platinum crucibles. The sample mass is determined by the size of the Pt crucibles and other properties of the heating apparatus and is chosen to avoid spattering and sample loss during fusion. For the set of samples with expected high ^{10}Be concentration, we added 400 μg of ^9Be carrier to each 0.5-g sample. This ^9Be carrier is a
115 beryl carrier (termed Carrier C) made at the facility with a concentration of 348 $\mu\text{g}/\text{mL}$. After drying the sample and carrier mixture, anhydrous KHF_2 and anhydrous Na_2SO_4 were added at the ratio of 8:1:2 KHF_2 : Na_2SO_4 :sample by weight to the crucibles and homogenized.

The fusion protocol at the University of Vermont uses 30 mL platinum crucibles which for safety reasons and splatter
120 control, limits sample size to 0.5 g. While it is possible to fuse larger (1-2 g) samples in larger (100 ml) crucibles (Stone, 1998), these are not compatible with the fixed fluxing apparatus used to minimize the hazard of molten KHF_2 . To increase the sample size and the measured $^{10}\text{Be}/^9\text{Be}$ ratio for the set of expected low ^{10}Be concentration samples, we fused 1 g of sample in two separate fusions of 0.5 g each, with half as much carrier (200 μg) as used for the initial sample batch. With
125 sample and carrier concentrations similar in both aliquots (specifically, as close as possible with the weighing and dispensing equipment in use; we estimate better than 1% agreement between aliquots), $^{10}\text{Be}/^9\text{Be}$ ratios in both aliquots after fusion can be expected to be identical, so we combined them to yield a higher sample/carrier ratio than possible in a single fusion.

Before starting this procedure, we determined whether halving the amount of ^9Be carrier would affect the Be yield, by fusing aliquots of sample 15-OTW-60 with varying amounts of added ^9Be carrier. Total ^9Be yields (Table 2) show that less ^9Be
130 does not result in a lower Be yield. Because Be yields in the first set of samples were lower than expected, we increased the amount of Na_2SO_4 added to a ratio of 4:2:1 KHF_2 : Na_2SO_4 :sample by weight as suggested for calcium-rich samples by Stone (1998). This change makes sense because the Ferrar pyroxene is calcic; having an abundance of SO_4 during fluxing suppresses the formation of CaBeF_4 , which is less soluble. This modification significantly increased the total Be yield (Table 2).

135

After fusion, the Stone (1998) procedure involves Be and K extraction by water leaching, and removal of residual fluorides by centrifuging. At this point, the two aliquots of each sample were combined, and K was removed from the combined



sample by precipitation of KClO_4 , evaporation of the supernatant to remove the remaining HClO_4 , and redissolution in 12 mL of dilute HNO_3 .

140

At this point, we experienced difficulty in completely redissolving the precipitated sample and found it necessary to centrifuge the sample multiple times to remove what we presumed to be the remaining KClO_4 . Although Be yields from these samples were as expected (Table 2), the resulting AMS targets had unusually low beam currents (given the fraction of beam current of other samples), which made AMS measurement more difficult than expected. We hypothesize that this is most likely the result of K carryover in the final stages of the extraction process and that this could have been prevented by increasing the volume of the final HNO_3 solutions to dissolve K more effectively.

145

Ratios of $^{10}\text{Be}/^9\text{Be}$ were measured at Lawrence Livermore National Laboratory (LLNL) and normalized to the 07KNSTD3110 standard (Nishiizumi et al., 2007) with a $^{10}\text{Be}/^9\text{Be}$ ratio of 2.85×10^{-12} . Uncertainties in calculated ^{10}Be concentrations include AMS measurement uncertainties, uncertainty on the Be carrier concentration, and uncertainty in blank corrections (Table 2). Five procedural blanks measured with both sample batches had a mean and standard deviation of 128000 ± 67000 atoms ^{10}Be . This is less than 0.4% of the total amount of ^{10}Be measured in any of the samples in the high-concentration batch (Table 2), so blank correction uncertainty makes a negligible contribution to overall measurement uncertainty for these samples. However, the highest blank values were up to 60% of the total number of atoms measured in some of the low-concentration samples, so blank uncertainty is significant for the low-concentration batch. We discuss this in more detail in section 3.5.

150

155

2.4 Cosmogenic ^3He Analysis

We measured cosmogenic ^3He concentrations in all samples at Berkeley Geochronology Center (BGC) following the procedure described in Balter-Kennedy et al. (2020). ^3He concentrations for two samples, HB-TC-02 and HB-TC-12, have already been reported in Stutz et al. (2021). Measurements of the CRONUS-P intercomparison standard (Blard et al., 2015) during the period of these measurements were $5.03 \pm 0.15 \times 10^9$ atoms g^{-1} ^3He (Balter-Kennedy et al., 2020), which is indistinguishable from the accepted value of $5.02 \pm 0.12 \times 10^9$ atoms g^{-1} (Blard et al., 2015).

160

3 Results and Discussion

3.1 Measured cosmogenic ^{10}Be in saturated samples.

Measured ^{10}Be concentrations in the set of high-concentration samples range from $5.92 - 7.67 \times 10^7$ atoms g^{-1} with uncertainties $< 2.2\%$ (Tables 2 and 3). These are equivalent to some of the highest ^{10}Be concentrations measured in terrestrial rocks (Spector and Balco, 2020). As expected from the elevation dependence of the ^{10}Be production rate and the

165



assumption that the ^{10}Be concentrations are close to production-decay saturation, the measured concentrations increase systematically with elevation (Fig. 1).

170



Table 2 Measure Be results, including yields measured by ICP-OES in the dilute HNO₃ solution prior to final precipitation, with implied Be yields for the fusion process and measured AMS current and ratios.

Sample Name	Pyroxene Mass (g)	⁹ Be Added (μg)	Be Yield (μg)	Be Yield (%)	AMS ¹⁰ Be/ ⁹ Be	Mean ⁹ Be current Relative to standard ^a	Measured ¹⁰ Be (10 ⁶ atoms)	Blank corr. ¹⁰ Be Conc. (10 ⁶ atoms g ⁻¹)
<i>High-concentration batch</i>								
15-ROB-07	0.493	403	110	27	1.281 ± 0.024 x 10 ⁻¹²	0.48	34.89 ± 0.75	70.5 ± 1.5
15-ROB-27	0.497	403	118	29	1.085 ± 0.018 x 10 ⁻¹²	0.54	29.57 ± 0.56	59.2 ± 1.1
15-ROB-30	0.488	402	145	36	1.222 ± 0.023 x 10 ⁻¹²	0.55	33.21 ± 0.7	67.8 ± 1.4
15-ROB-31	0.501	400	132	33	1.192 ± 0.018 x 10 ⁻¹²	0.66	32.21 ± 0.59	64 ± 1.2
15-OTW-50	0.498	398	117	30	1.165 ± 0.022 x 10 ⁻¹²	0.59	31.34 ± 0.67	62.7 ± 1.3
15-OTW-55	0.496	402	117	29	1.139 ± 0.021 x 10 ⁻¹²	0.47	30.96 ± 0.66	62.2 ± 1.3
15-OTW-56	0.498	399	108	27	1.232 ± 0.023 x 10 ⁻¹²	0.53	33.23 ± 0.7	66.5 ± 1.4
15-OTW-57	0.490	397	113	28	1.182 ± 0.022 x 10 ⁻¹²	0.60	31.71 ± 0.67	64.5 ± 1.4
15-OTW-58	0.501	399	107	27	1.429 ± 0.028 x 10 ⁻¹²	0.50	38.56 ± 0.85	76.7 ± 1.7
15-OTW-60	0.497	398	114	29	1.369 ± 0.026 x 10 ⁻¹²	0.47	36.87 ± 0.78	73.9 ± 1.6
15-OTW-60-150 ^b	0.493	159	64	40	-	-	-	-
15-OTW-60-250 ^b	0.495	258	79	31	-	-	-	-
Blank (129-BLK)	-	398	279	70	5.1 ± 1 x 10 ⁻¹⁵	0.80	0.139 ± 0.028	-
Blank (129-BLKX)	-	404	267	66	5.28 ± 0.48 x 10 ⁻¹⁵	0.62	0.144 ± 0.013	-
Blank (129-0BLK)	-	402	297	74	2.18 ± 0.27 x 10 ⁻¹⁵	0.79	0.0594 ± 0.0074	-
<i>Low-concentration batch</i>								
17-HB-TC-02	0.998	400	268	67	2.53 ± 0.11 x 10 ⁻¹⁴	0.49	0.685 ± 0.03	0.558 ± 0.074
17-HB-TC-12	0.997	400	250	63	2.03 ± 0.11 x 10 ⁻¹⁴	0.36	0.55 ± 0.03	0.424 ± 0.074
17-EHW-05	0.998	399	242	61	1.67 ± 0.13 x 10 ⁻¹⁴	0.22	0.451 ± 0.034	0.323 ± 0.075
17-EHW-15	0.999	399	267	67	3.70 ± 0.17 x 10 ⁻¹⁴	0.27	0.997 ± 0.046	0.87 ± 0.082
15-MG12	1.001	398	281	71	2.40 ± 0.13 x 10 ⁻¹⁴	0.32	0.646 ± 0.037	0.517 ± 0.076
15-MG19	1.000	399	263	66	3.96 ± 0.55 x 10 ⁻¹⁴	0.10	1.07 ± 0.15	0.94 ± 0.16
Blank (130-BLK)	-	399	333	83	8.3 ± 1.2 x 10 ⁻¹⁵	0.17	0.226 ± 0.032	-
Blank (130-BLKX)	-	399	333	83	2.62 ± 0.54 x 10 ⁻¹⁵	0.25	0.071 ± 0.015	-

^a Mean current for the KNSTD3110 is 21.5 μA

^b Sample were processes only as a yield test and no AMS measurements were made



Table 3. ^3He and ^{10}Be concentrations for long-exposed glacial erratics in the Transantarctic Mountains. The ^{10}Be production rate is determined from Eq. 1.

Sample ID	^{10}Be conc. (10^9 atoms g)	^3He conc. (10^9 atoms g)	^3He exposure age (Myrs)	^{10}Be production rate SLHL spallation ^a (atoms g^{-1} yr^{-1})	^3He data from
15-ROB-07	7.05 ± 0.15	9.19 ± 0.18	8.12 ± 0.16	4.26	Balter-Kennedy et al., (2020)
15-ROB-27	5.92 ± 0.11	9.05 ± 0.10	8.265 ± 0.094	3.69	Balter-Kennedy et al., (2020)
15-ROB-30	6.78 ± 0.14	12.21 ± 0.35	9.95 ± 0.29	3.78	Balter-Kennedy et al., (2020)
15-ROB-31	6.40 ± 0.12	10.51 ± 0.14	8.67 ± 0.12	3.62	Balter-Kennedy et al., (2020)
15-OTW-50	6.27 ± 0.13	10.84 ± 0.26	9.40 ± 0.23	3.68	ICE-D Database ^b
15-OTW-55	6.22 ± 0.13	11.07 ± 0.13	9.56 ± 0.11	3.64	ICE-D Database ^c
15-OTW-56	6.65 ± 0.14	10.53 ± 0.13	9.14 ± 0.12	3.92	ICE-D Database ^c
15-OTW-57	6.45 ± 0.14	10.87 ± 0.16	9.28 ± 0.13	3.74	ICE-D Database ^c
15-OTW-58	7.67 ± 0.17	12.4235 ± 0.0092	9.0549 ± 0.0067	3.88	ICE-D Database ^c
15-OTW-60	7.39 ± 0.16	11.73 ± 0.23	8.54 ± 0.17	3.74	ICE-D Database ^c

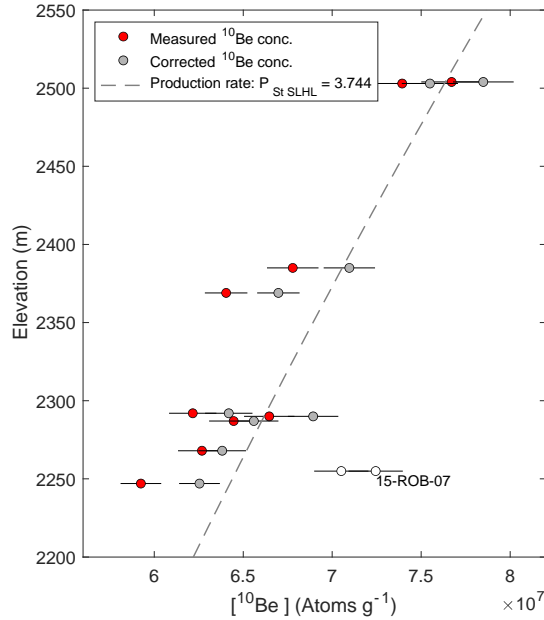
^a The reference ^{10}Be production rate is determined from Equation (1) and the scaling method of Stone (2000), as implemented Balco et al., (2008)

^b <https://version2.ice-d.org/antarctica/site/CHARLIE/>

^c <https://version2.ice-d.org/antarctica/site/OTWEBAS/>



180



185

Figure 1: Measured ^{10}Be concentrations versus elevation. Red dots are measured ^{10}Be concentrations as reported in Table 3, gray dots show measured ^{10}Be concentrations corrected for sample thickness and shielding, and dashed line show the saturated ^{10}Be concentrations for the ‘St’ reference production rate of $3.74 \text{ atoms g}^{-1} \text{ yr}^{-1}$ ^{10}Be in pyroxene. White dots indicate sample outlier, which is not included in the production rate calibration (see section 3.2).

3.2 ^{10}Be Production rate in pyroxene

In general, as discussed above, ^3He exposure ages range between 8-10 Ma (5-6 times the ^{10}Be half-life) and imply that ^{10}Be concentrations in these samples are within 1-2% of production-decay saturation. We account for the small, predicted difference from the saturation concentration by calculating the production rate as,

190

$$P_{10} = \frac{N_{10} \lambda_{10}}{(1 - e^{-\lambda_{10} t_3})}, \quad (1)$$

195

where N_{10} is the ^{10}Be concentration (atoms g^{-1}), P_{10} is the ^{10}Be production rate in the sample (atoms $\text{g}^{-1} \text{ yr}^{-1}$), λ_{10} is the ^{10}Be decay constant ($4.99 \times 10^{-7} \text{ yr}^{-1}$), and t_3 is the ^3He exposure age (yr). Because the samples are close to production-decay saturation, the production rate determined from Eq. 1 is insensitive to uncertainty in the assumed exposure age. Therefore, although we use the apparent ^3He exposure ages to correct for an inferred small systematic difference from production-decay saturation, the accuracy of the ^3He ages is minimally important for the ^{10}Be production rate estimate. To obtain the



spallogenic production rate of ^{10}Be in pyroxene, we subtract the production rate in pyroxene due to muons using the muon interaction cross-sections of Balter-Kennedy et al. (2023) and correct for sample thickness and topographic shielding.

200

Applying the ‘St’ elevation scaling of Stone (2000) then yields sea level/high latitude (SLHL) production rates in the range of 3.5-4.1 atoms $\text{g}^{-1} \text{yr}^{-1}$ (Table 3). The ^{10}Be production rate increases with elevation, so samples near or at saturations are expected to likewise have ^{10}Be concentrations increase with elevation. This is true for all samples, except 15-ROB-07, which have an excess ^{10}Be concentrations equivalent to ~250 m (Fig. 1). Removing one outlier (15-ROB-07, see Fig. 1) yields a

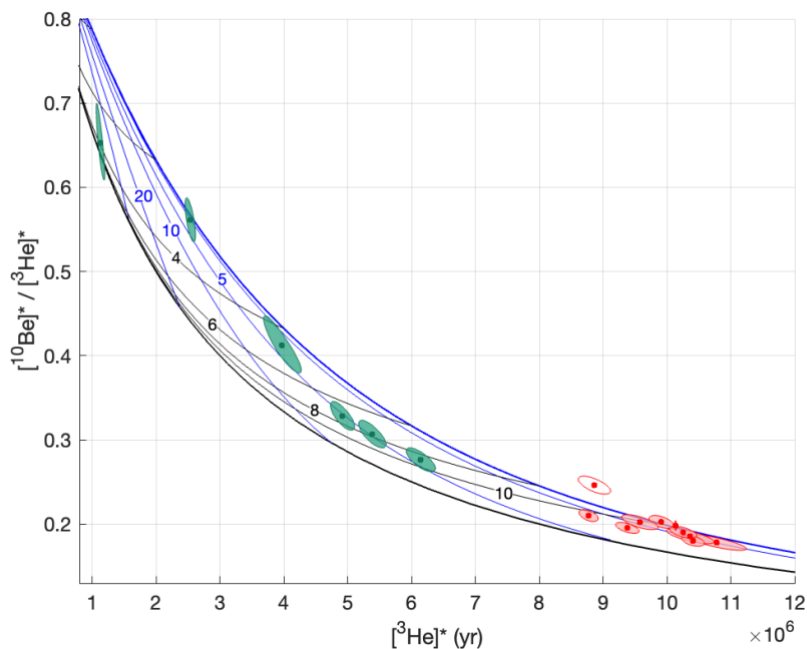
205

The production rate estimate agrees with that of Balter-Kennedy et al. (2023) (3.6 ± 0.2 atoms $\text{g}^{-1} \text{yr}^{-1}$). However, in this study, samples with near-saturated ^{10}Be concentrations permit a direct calculation of the production rate from the measurements. In contrast, the sample set in the Balter-Kennedy et al. (2023) study lacks direct constraints on the exposure age and/or exposure history, and a best-fit production rate was computed from values that permitted all the samples to have a simple exposure history bounded by limiting assumptions of steady exposure at zero erosion and steady erosion for an infinite time. While they are not directly comparable, it is possible to determine whether the two data sets are consistent with each other and with the assumption of simple exposure. In Fig. 2 we construct a $^{10}\text{Be}/^3\text{He}$ two-nuclide diagram using the production rate determined from our study and plot the $^{10}\text{Be}/^3\text{He}$ data from both studies. This shows that all data from both

210

215

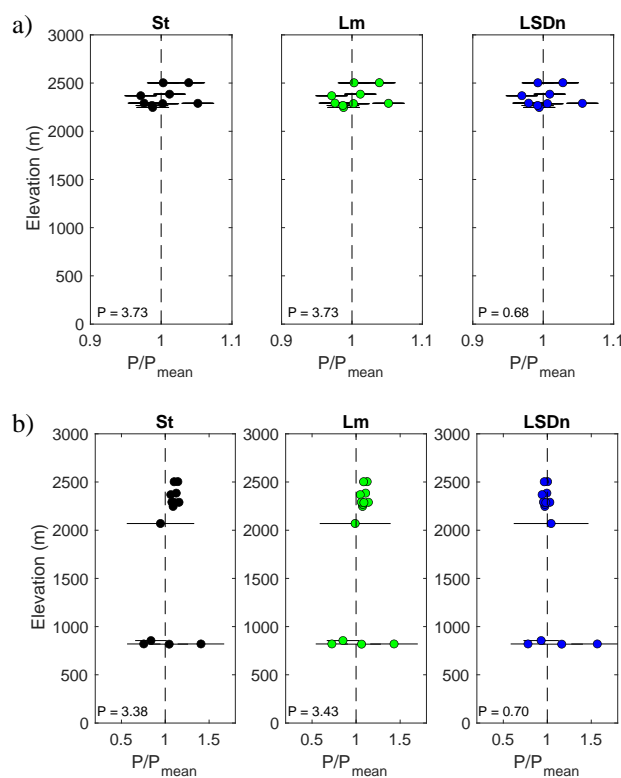
internally consistent.



220 **Figure 2:** ^{10}Be - ^3He two-nuclide diagram. Red data points show measurements from this study, green data are from Balter-Kennedy et al., (2023), where each shaded ellipse represents the 68% confidence interval in the measured uncertainty. Thick blue line is the simple exposure line and the thin blue lines are lines of constant erosion (m Myr^{-1}). Thick black is the steady-erosion line, and the thin black lines are constant age (Myr). * signifies nuclide concentrations normalized to site-specific production rate for comparison across sampling locations.

225 Finally, we consider whether our data are consistent with other ^{10}Be -in-pyroxene production rate calibration data and with commonly used production rate scaling methods. Two other studies obtained ^{10}Be -in-pyroxene production rate calibration data from samples with independent age constraints. Blard et al. (2008) included two samples (SI41 and SI43) from separate lava flows at Mt. Etna, Italy with K/Ar ages of 33 kyrs and 10 kyrs, respectively. Eaves et al. (2018) obtained three samples from the Murimotu formation debris avalanche at Mt Ruapehu, New Zealand, which has a radiocarbon age of 10.5 kyrs.

230 In Fig. 3, we apply the production rate calibration code from version 3 of the online exposure age calculator originally described by Balco et al. (2008) and subsequently updated, to (i) our production rate calibration data alone, and (ii) our data with the Blard et al. (2008) and Eaves et al. (2018) data. One potentially important aspect of this comparison is that our data are from relatively high elevations and high latitudes, and the other calibration data are from relatively low elevations and moderate latitudes. Therefore, this comparison is a potential test of the hypothesis that the time-dependent ‘LSDn’ scaling method (Lifton et al., 2014; Lifton, 2016) more accurately represents the elevation dependence of the production rate at high latitudes (Balco, 2016). In fact, Fig. 3 shows that, in agreement with this hypothesis, LSDn scaling suppresses an elevation-dependent residual in reference production rates calculated with the ‘St’ and ‘Lm’ scaling methods.



240

Figure 3: Relative variation with elevation in production rate scaling parameters calculated from calibration samples in this study (high-elevation data; shown in both panels (a) and (b)) and those of Blard et al. (2008) and Eaves et al. (2018) (lower-elevation data; shown in panel (b) only). For the St and Lm scaling methods, the production rate scaling parameter P is a reference production rate with units of atoms $\text{g}^{-1}\text{yr}^{-1}$; for the LSDn scaling method, it is a nondimensional correction factor. An elevation-dependent residual is evident for St and Lm scaling but is resolved by LSDn scaling. This implies that LSDn scaling better represents the elevation dependence of the production rate at polar latitudes.

245

Taken all together, we find that the reference production rate of 3.74 ± 0.10 atoms $\text{g}^{-1}\text{yr}^{-1}$ determined in this study is in agreement with previously published production rates of 3.6 ± 0.2 atoms $\text{g}^{-1}\text{yr}^{-1}$ with an overall improvement in the uncertainty.

250 3.3 ^{10}Be and ^3He measurements in low-concentration samples

The ^{10}Be concentrations from the set of young-exposure-age erratics, as expected, were two orders of magnitude lower than concentrations in the high-elevation, saturated samples (Table 4). As discussed above, these samples are glacially transported erratics found near the margins of major glaciers in the Transantarctic Mountains. The geomorphic context, ^3He exposure ages on these and nearby samples, and ^{10}Be exposure ages on nearby quartz-bearing samples, all indicate that these samples



255 were emplaced by deglaciation during the last glacial-interglacial cycle and have most likely not experienced more than
50,000 years of exposure (Stutz et al., 2021; Eaves et al., 2018).

Given the assumptions that (i) the samples have experienced exposure only in the last ~50,000 years and (ii) the non-
cosmogenic ^3He concentration is constant among samples, measured ^3He and ^{10}Be concentrations should be linearly related,
260 with a slope given by the $^3\text{He}/^{10}\text{Be}$ production ratio and an intercept on the ^3He axis given by the non-cosmogenic ^3He
concentration in Ferrar pyroxene. Non-cosmogenic ^3He in Ferrar pyroxene is most likely derived from nucleogenic
production and has been estimated in various studies to be less than approximately 6 Matoms g^{-1} (Ackert, 2000; Kaplan et
al., 2017; Margerison et al., 2005).

265 Combining our ^3He measurements with the ^{10}Be concentrations obtained from Collins (2015) and Eaves et al. (2018) results
in the expected linear relationship, with a slope of $^3\text{He}/^{10}\text{Be} = 28.5 \pm 4.6$ and ^3He intercept of $3.9 \pm 0.8 \times 10^6$ atoms g^{-1} . If we
take the reference ^3He production rate to be 120 ± 13 atoms $\text{g}^{-1} \text{yr}^{-1}$, which is derived for 'St' scaling with the calibration data
set of Borchers et al., (2016), this slope implies a ^{10}Be production rate of 4.20 ± 0.82 atoms $\text{g}^{-1} \text{yr}^{-1}$, which is consistent with,
although less precise than, the other estimates discussed in the previous sections. The ^3He intercept is most likely a good
270 estimate of the nucleogenic ^3He concentration in Ferrar pyroxene (Balco, 2020).

However, only one of the ^{10}Be concentrations measured in this study agrees with the expected linear relationship; the others
are systematically higher than expected, by hundreds of thousands of atoms g^{-1} . In particular, MG12 and MG19 were
measured both by Eaves et al., (2018) and in this study; our results are 3.94×10^5 and 8.4×10^5 atoms g^{-1} higher than the
275 Eaves et al., (2018) results, respectively (Table 4). Two possible explanations for this discrepancy are (i) failure to
completely remove meteoric $^{10}\text{Be}_m$ before extraction, or (ii) a highly variable and poorly quantified measurement
background (Table 2). Both scenarios are discussed in the following sections.



Table 4 Measured ^3He and ^{10}Be concentrations in low-concentration samples from glacial transported erratics during the last glacial-interglacial cycle, including published concentrations from others.

Sample name	aliquot	Mass (g)	Measured ^4He (10^9 atoms g^{-1})	Total Measured ^3He (10^6 atoms g^{-1})	Total ^3He weighted mean (10^6 atoms g^{-1})	^3He data source	Measured ^{10}Be (10^6 atoms g^{-1})	^{10}Be data source	
<i>Mr. Gram (Mackay Glacier)</i>									
MG-01	a	0.03887	34.3 ± 1.2	5.88 ± 0.77	6.36 ± 0.42	This paper	0.055 ± 0.040	Eaves et al. (2018)	
	b	0.09641	35.3 ± 1.3	6.56 ± 0.50					
MG-02B	a	0.04679	159.1 ± 5.7	8.40 ± 0.85	8.26 ± 0.48	This paper	0.271 ± 0.062	Collins (2015)	
	b	0.08192	158.4 ± 5.6	8.15 ± 0.69					
	c	0.04119	154.6 ± 5.6	8.31 ± 1.06					
MG-07	a	0.06049	34.7 ± 1.2	14.13 ± 0.80	14.13 ± 0.80	This paper	0.337 ± 0.087	Eaves et al. (2018)	
MG-08B	b	0.01779	131.1 ± 4.7	22.27 ± 2.40	19.13 ± 1.12	This paper	0.52 ± 0.10	Collins (2015)	
	c	0.04954	295.4 ± 10.6	18.26 ± 1.26					
MG-15	a	0.09931	84.9 ± 3	8.52 ± 0.63	7.77 ± 0.46	This paper	0.182 ± 0.048	Eaves et al. (2018)	
	b	0.07935	81.3 ± 2.9	6.90 ± 0.67					
MG-22	a	0.09661	29.1 ± 1	7.34 ± 0.61	7.28 ± 0.53	This paper	0.093 ± 0.036	Eaves et al. (2018)	
	b	0.03488	28.1 ± 1	7.10 ± 1.05					
MG-32	a	0.09666	36.5 ± 1.3	9.99 ± 0.62	9.54 ± 0.53	This paper	0.135 ± 0.051	Eaves et al. (2018)	
	b	0.03643	38 ± 1.4	8.34 ± 1.01					
MG-12	a	0.02253	174.1 ± 1.5	7.29 ± 0.88	6.56 ± 1.02	This paper	0.123 ± 0.034	Eaves et al. (2018)	
	b	0.01526	243.9 ± 2.1	5.40 ± 1.62					
	c	0.02199	165.4 ± 1.4	6.98 ± 0.87					
MG-19	a	0.02329	583.7 ± 4.9	7.16 ± 1.02	7.78 ± 2.32	This paper	0.517 ± 0.076	This paper	

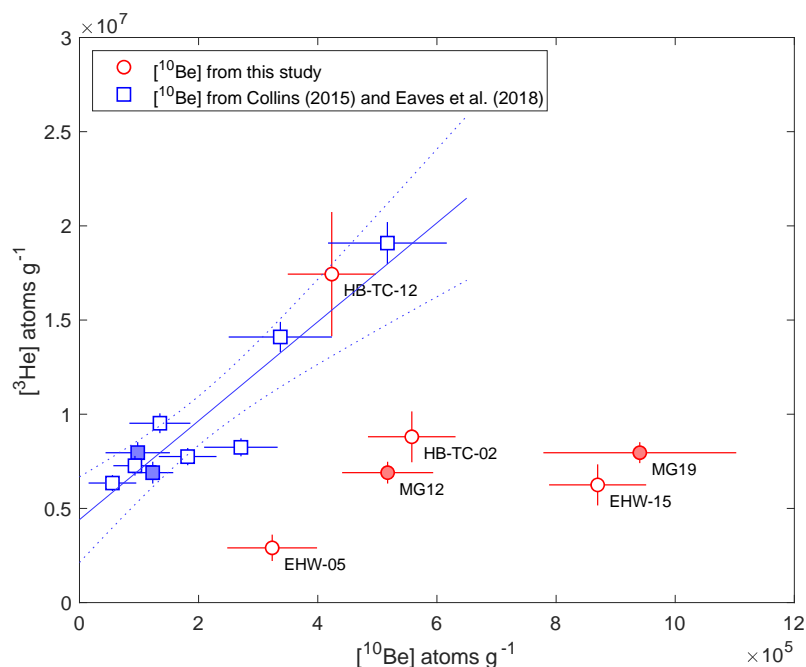


	c	0.02600	590.9 ± 4.9	10.66 ± 1.05				
	d	0.01643	602.0 ± 4.9	6.02 ± 1.32				
	e	0.01431	525.2 ± 4.4	9.74 ± 1.66				
	f	0.01403	490.1 ± 4.1	5.34 ± 1.50				
<i>Evans Heights (David Glacier)</i>								
EHW-05	a	0.02364	108.6 ± 1.8	3.76 ± 1.67	2.91 ± 0.7	This paper		
	b	0.06775	108.0 ± 1.9	4.43 ± 0.87				
	c	0.05934	107.7 ± 1.9	1.60 ± 0.75				
EHW-15	a	0.02905	216.5 ± 3.7	6.91 ± 1.46	6.3 ± 1.1	This paper	0.323 ± 0.075	This paper
	b	0.03577	179.9 ± 3.1	4.43 ± 1.40				
	c	0.03328	178.3 ± 3.1	7.73 ± 1.52				0.87 ± 0.082
<i>Hughes Bluff (David Glacier)</i>								
HB-TC-02	a	0.02268	230.0 ± 5.5	11.85 ± 2.08	8.8 ± 1.4	Stutz et al. (2021)		
	b	0.03491	195.9 ± 3.4	8.16 ± 1.73				
	c	0.03291	178.9 ± 3.1	7.49 ± 1.67				0.558 ± 0.074
HB-TC-12	c	0.01439	99.2 ± 1.7	17.48 ± 3.31	17.5 ± 3.3	Stutz et al. (2021)		This paper
							0.424 ± 0.074	This paper

Notes:

1. All ^3He measurements employed the BGC "Ohio" NGMS system. Analytical methods are as described in Baller-Kennedy et al., (2020)
2. ^{10}Be data from Eaves and Collins were originally normalized to the NIST SRM4325 standard with an assumed $^{10}\text{Be}/^9\text{Be}$ ratio of 3×10^{-11} , and have been renormalized to the '07KNSTD' standardization of Nishizumi et al., (2007).

280

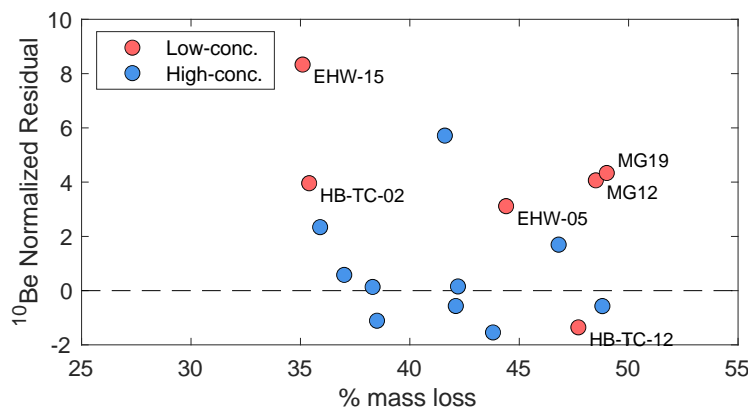


285 **Figure 4: Measured ^{10}Be and ^3He concentrations in low-concentration samples. Red dots are sample data with ^{10}Be concentrations measured in this study. Blue squares are sample data with ^{10}Be concentrations obtained from Collins (2016) and Eaves et al., (2018). Solid points represent samples having duplicated ^{10}Be measurements from this study and Eaves et al., (2018). The horizontal and vertical lines associated with each data point are the measured uncertainty in the nuclide concentrations. Blue solid line is the linear relationship for the blue data points only with a 95% confidence bound (dashed blue lines).**

3.4 Removal of meteoric ^{10}Be

290 Failure to successfully remove all meteoric $^{10}\text{Be}_m$ during HF etching would result in spuriously high concentrations of presumed cosmogenic ^{10}Be . Balter-Kennedy et al. (2023) found that when using fine to medium grains of pyroxene (32-125 μm), ~25% mass loss after leaching a sample in 1% HF/1% HNO_3 is sufficient to remove meteoric $^{10}\text{Be}_m$. After leaching, we observed 35–49% mass loss, indicating that leaching should have been sufficient. Figure 5 compares the mass lost during HF etching to the normalized residual between the measured and predicted cosmogenic ^{10}Be concentration (atoms g^{-1}) calculated using the production rate from this study of 3.74 atoms $\text{g}^{-1} \text{yr}^{-1}$ and the minimum ^3He ages for both the high- and low-concentration samples. We see no clear relationship between mass loss and the ^{10}Be residual for either of the two sample sets, as expected. This is especially evident in samples HB-TC-12 and MG19 which both display similar mass loss (~48%).

295



300 **Figure 5: Comparison of mass lost during HF etching prior to ¹⁰Be extraction and the normalized residual between measured and predicted cosmogenic ¹⁰Be concentrations. Red data points are from the sample set of low ¹⁰Be concentrations. Blue data points are from the sample set having high ¹⁰Be concentrations.**

If we were to assume that the increased ¹⁰Be is solely meteoric, then that contributes $\sim 6 \times 10^5$ atoms g^{-1} , which is estimated from the average difference between the ¹⁰Be concentrations for the replicated samples. This would account for less than 1% of the ¹⁰Be concentration measured for the set of high-concentration samples used for estimating the production rate of ¹⁰Be in pyroxene. Therefore, any potential contribution from meteoric ¹⁰Be would most likely have an insignificant impact on the reference production rate reported in section 3.2.

As dissolved plagioclase attached to pyroxene grains contributes to the total mass loss after leaching, the total mass loss is not a direct reflection of the mass of pyroxene lost and presumed to contain meteoric ¹⁰Be_m. While the >35% mass loss is mostly pyroxene, some unknown fraction could be from plagioclase. We can therefore not exclude that samples may contain some meteoric ¹⁰Be_m. However, the lack of correlation between the residuals vs. expected values and the mass loss during etching makes it unlikely that the systematically measured increase in ¹⁰Be concentration is solely caused by meteoric ¹⁰Be_m.

3.5 Uncertainty in the blank correction.

The blank correction may be one of the major challenges for analyzing low ¹⁰Be concentration samples, and a highly variable blank could cause a scatter and increase in measured ¹⁰Be concentrations that we observed. The blank correction value is obtained from the average of all five blanks processed during both the high- and low-concentration sample sets. However, the blanks are highly variable between 71,000 and 288,000 ¹⁰Be atoms, which accounts for 10-60 % of the total measured ¹⁰Be atoms in the low-concentration batch. If, for sample HB-TC-02, we assume a blank of 71000 ¹⁰Be atoms, we get a corrected ¹⁰Be concentration of 6.15×10^5 atoms g^{-1} . However, if we assume a blank of 288,000 ¹⁰Be atoms, we get a ¹⁰Be concentration of 3.97×10^5 atoms g^{-1} , a significantly lower ¹⁰Be concentration. Thus, variability in the measurement background may account for a significant fraction of the difference between measured and expected concentrations. It would



only be possible to quantify this contribution of ^{10}Be by measuring additional blanks as well as replicates of low-concentration samples.

3.6 Limitations in extracting cosmogenic ^{10}Be from Pyroxene by fusion.

325 Agreement of our production rate estimate from saturated samples with all other existing data shows that extraction of
cosmogenic ^{10}Be from pyroxene by total rapid fusion is effective and accurate for samples with high ^{10}Be concentrations.
Previous studies of ^{10}Be in pyroxene used wet chemical dissolution and ion exchange chromatography, similar to the
procedure used in extracting ^{10}Be from quartz. However, concentrations of the major cations Ca, Fe, Mg, and Na are much
greater in pyroxene than the trace levels found in quartz, which requires substantial scaling up of ion exchange columns
330 (Eaves et al., 2018). The total fusion method of Stone (1998), having extremely high selectivity for Be relative to these
cations, completely avoids this issue. However, we were not able to sufficiently scale up the rapid fusion method to obtain
the desired signal/noise ratio during AMS analysis for the lower-concentration samples.

3.6.1 Sample Size Limitations.

335 The main obstacle to measuring cosmogenic ^{10}Be in pyroxene at low concentrations is the difficulty in increasing the sample
size to obtain a higher $^{10}\text{Be}/^9\text{Be}$ ratio and thus signal/background ratio. This is a challenge for both extraction methods,
although for different reasons. For young exposure age samples (5-33 kyrs), Eaves et al. (2018) dissolved 1.1-2.8 g of
pyroxene using large ion exchange columns. For our extraction by total fusion, the sample size is limited to 0.5 g by the size
of the Pt crucibles. Note that Stone (1998) processed samples up to 4 g using 100 mL crucibles.

340 As discussed above, to address the crucible size limitation, we merged duplicate samples of 0.5 g to obtain a total sample
mass of 1 g, but increasing the amount of K present in the final steps of the procedure most likely resulted in incomplete
separation of K from Be. This, in turn, may have suppressed AMS beam currents (Table 2) and resulted in poor
measurement precision for some samples. This could likely be corrected by increasing solution volumes in some steps of the
procedure and repeating various precipitation steps to ensure the complete removal of K.

345

Conclusion

In this study we provide advances in the measurement and application of cosmogenic ^{10}Be in pyroxene, by applying a rapid
fusion extraction method (Stone, 1998) and a production rate calibration data set. We extracted and measured cosmogenic
 ^{10}Be in pyroxene from two sets of Ferrar Dolerite samples. One set of samples consisting of 10 high-elevation boulders
350 collected from moraines in the upper TAM have ^3He measurements indicating that these samples have ^{10}Be concentration
close to saturation. We use this sample set to calibrate the production rate of ^{10}Be in pyroxene by assuming production-
erosion equilibrium. The other set of samples consisting of 6 low-elevation glacially transported erratics from Northern

Victoria Land are used to test whether or not a rapid fusion extraction method is feasible for samples having low ^{10}Be concentrations.

355

From measured ^{10}Be concentrations in the near-saturation sample set we find the production rate of ^{10}Be in pyroxene to be 3.74 ± 0.10 atoms $\text{g}^{-1} \text{yr}^{-1}$ which is in agreement with previously published production rate, and consistent with $^{10}\text{Be}/^3\text{He}$ paired nuclide ratios from samples assumed to have simple exposure. Given the high ^{10}Be concentration measured, a sample mass of ~ 0.5 g of pyroxene with 400 μg added ^9Be carrier is sufficient for obtaining meaningful $^{10}\text{Be}/^9\text{Be}$ ratios well above blank levels. Even with relatively low Be yields, there is still enough total Be present for AMS detection. Therefore, the extraction of cosmogenic ^{10}Be from pyroxene samples using rapid fusion works well for samples with high ^{10}Be concentrations. However, for the sample set having low ^{10}Be concentrations, the measured concentrations are higher than expected by 320,000 – 810,000 atoms g^{-1} . We contribute this increased ^{10}Be concentration to potential failure in completely removing all meteoric ^{10}Be and/or a highly variable and poorly quantified measurement background.

365

Advances in measuring ^{10}Be in pyroxene and constraints on the production rate provide new opportunities for multi-nuclide measurement in pyroxene-bearing samples that allow for correcting exposure ages for surface weathering and erosion and establishing exposure-burial history.

370 **Code and data availability** All data information associated with the cosmogenic nuclide measurements appears in tables. The exposure age and production rate calibration in the online exposure age calculator version 3 (Balco et al., 2008) has been updated to accept data from ^{10}Be in pyroxene.

375 **Author Contribution** MB carried out sample preparation for unprocessed samples. MB and LBC performed beryllium extraction. MB and GB performed helium analysis, data reduction, and all data analysis. MB prepared the manuscript with contributions from all authors.

Competing interests Greg Balco is an editorial board member of Geochronology.

380 **Acknowledgements** We would like to thank Allie Balter-Kennedy, Shaun Eaves, and Jamey Stutz for kindly providing the samples used for this study. Further, we thank Alan Hidy of the Center for Accelerator Mass Spectrometry, Lawrence Livermore National Laboratory for Beryllium measurements. This project was supported by the U.S. National Science Foundation via grants OPP- 2139497. The LLNL portion of this work was carried out under Contract DE-AC52-07NA27344. This is LLNL-JRNL-XXXX-DRAFT.



385 References

- Ackert, R. P.: Antarctic glacial chronology: new constraints from surface exposure dating, Massachusetts Institute of Technology and Woods Hole Oceanographic Institution, Woods Hole Open Access Server, 10.1575/1912/4123, 2000.
- Balco, G.: Saturated surfaces in Antarctica. The bleeding edge of cosmogenic-nuclide geochemistry. <https://cosmognosis.wordpress.com/2016/09/09/saturated-surfaces-in-antarctica/>, 2016.
- 390 Noncosmogenic helium-3 in pyroxene and Antarctic exposure dating, last access: 21 January.
- Balco, G. and Rovey, C. W.: An isochron method for cosmogenic-nuclide dating of buried soils and sediments, *American Journal of Science*, 308, 1083-1114, 10.2475/10.2008.02, 2008.
- Balco, G. and Shuster, D. L.: Production rate of cosmogenic ^{21}Ne in quartz estimated from ^{10}Be , ^{26}Al , and ^{21}Ne concentrations in slowly eroding Antarctic bedrock surfaces, *Earth and Planetary Science Letters*, 281, 48-58, 10.1016/j.epsl.2009.02.006, 2009.
- 395 Balco, G., Stone, J. O., Lifton, N. A., and Dunai, T. J.: A complete and easily accessible means of calculating surface exposure ages or erosion rates from ^{10}Be and ^{26}Al measurements, *Quaternary Geochronology*, 3, 174-195, 10.1016/j.quageo.2007.12.001, 2008.
- Balter-Kennedy, A., Bromley, G., Balco, G., Thomas, H., and Jackson, M. S.: A 14.5-million-year record of East Antarctic Ice Sheet fluctuations from the central Transantarctic Mountains, constrained with cosmogenic ^3He , ^{10}Be , ^{21}Ne , and ^{26}Al , *The Cryosphere*, 14, 2647-2672, 10.5194/tc-14-2647-2020, 2020.
- 400 Blard, P. H.: Cosmogenic ^3He in terrestrial rocks: A review, *Chemical Geology*, 586, 10.1016/j.chemgeo.2021.120543, 2021.
- Blard, P. H., Bourlès, D., Pik, R., and Lavé, J.: In situ cosmogenic ^{10}Be in olivines and pyroxenes, *Quaternary Geochronology*, 3, 196-205, 10.1016/j.quageo.2007.11.006, 2008.
- 405 Blard, P. H., Balco, G., Burnard, P. G., Farley, K. A., Fenton, C. R., Friedrich, R., Jull, A. J. T., Niedermann, S., Pik, R., Schaefer, J. M., Scott, E. M., Shuster, D. L., Stuart, F. M., Stute, M., Tibari, B., Winckler, G., and Zimmermann, L.: An inter-laboratory comparison of cosmogenic ^3He and radiogenic ^4He in the CRONUS-P pyroxene standard, *Quaternary Geochronology*, 26, 11-19, 10.1016/j.quageo.2014.08.004, 2015.
- 410 Borchers, B., Marrero, S., Balco, G., Caffee, M., Goehring, B., Lifton, N., Nishiizumi, K., Phillips, F., Schaefer, J., and Stone, J.: Geological calibration of spallation production rates in the CRONUS-Earth project, *Quaternary Geochronology*, 31, 188-198, 10.1016/j.quageo.2015.01.009, 2016.
- Collins, J. A.: In situ cosmogenic ^{10}Be in pyroxene with an application to surface exposure dating, School of Geography, Environment and Earth Sciences, Victoria University of Wellington, Victoria University of Wellington, 2015.
- 415 Corbett, L. B., Bierman, P. R., and Rood, D. H.: An approach for optimizing in situ cosmogenic ^{10}Be sample preparation, *Quaternary Geochronology*, 33, 24-34, 10.1016/j.quageo.2016.02.001, 2016.



- Eaves, S. R., Collins, J. A., Jones, R. S., Norton, K. P., Tims, S. G., and Mackintosh, A. N.: Further constraint of the in situ cosmogenic ^{10}Be production rate in pyroxene and a viability test for late Quaternary exposure dating, *Quaternary Geochronology*, 48, 121-132, 10.1016/j.quageo.2018.09.006, 2018.
- 420 Elliot, D. H. and Fleming, T. H.: Chapter 2.1b Ferrar Large Igneous Province: petrology, Geological Society, London, *Memoirs*, 55, 93-119, 10.1144/m55-2018-39, 2021.
- Granger, D. E.: A review of burial dating methods using ^{26}Al and ^{10}Be , *Special Paper of the Geological Society of America*, 415, 1-16, 10.1130/2006.2415(01), 2006.
- 425 Granger, D. E. and Muzikar, P. F.: Dating sediment burial with in situ-produced cosmogenic nuclides: theory, techniques, and limitations, *Earth and Planetary Science Letters*, 188, 269-281, 10.1016/S0012-821X(01)00309-0, 2001.
- Harvey, R. P.: The Ferra Dolerite: An Antarctic analog for martian basaltic lithologies and weathering processes, 2001.
- Ivy-Ochs, S., Kubik, P. W., Masarik, J., Wieler, R., Bruno, L., and Schluchter, C.: Preliminary results on the use of pyroxene for ^{10}Be surface exposure dating, *Schweizerische Mineralogische und Petrographische Mitteilungen*, 78, 375-382, 1998.
- 430 Jull, A. J. T., Donahue, D. J., Linick, T. W., and Wilson, G. C.: Spallogenic ^{14}C in High-Altitude Rocks and in Antarctic Meteorites, *Radiocarbon*, 31, 719-724, 10.1017/S0033822200012315, 1989.
- Kaplan, M. R., Licht, K. J., Winckler, G., Schaefer, J. M., Bader, N., Mathieson, C., Roberts, M., Kassab, C. M., Schwartz, R., and Graly, J. A.: Middle to Late Pleistocene stability of the central East Antarctic Ice Sheet at the head of Law Glacier, *Geology*, 45, 963-966, 10.1130/g39189.1, 2017.
- 435 Klein, J., Giegengack, R., Middleton, R., Sharma, P., Underwood, J. R., and Weeks, R. A.: Revealing Histories of Exposure Using In Situ Produced ^{26}Al and ^{10}Be in Libyan Desert Glass, *Radiocarbon*, 28, 547-555, 10.1017/S0033822200007700, 1986.
- Lal, D.: Cosmic ray labeling of erosion surfaces in situ nuclide production rates and erosion models, *Earth and Planetary Science Letters*, 104, 424-439, 10.1016/0012-821X(91)90220-C, 1991.
- 440 Lifton, N.: Implications of two Holocene time-dependent geomagnetic models for cosmogenic nuclide production rate scaling, *Earth and Planetary Science Letters*, 433, 257-268, 10.1016/j.epsl.2015.11.006, 2016.
- Lifton, N., Sato, T., and Dunai, T. J.: Scaling in situ cosmogenic nuclide production rates using analytical approximations to atmospheric cosmic-ray fluxes, *Earth and Planetary Science Letters*, 386, 149-160, 10.1016/j.epsl.2013.10.052, 2014.
- Margerison, H. R., Phillips, W. M., Stuart, F. M., and Sugden, D. E.: Cosmogenic ^3He concentrations in ancient flood deposits from the Coombs Hills, northern Dry Valleys, East Antarctica: interpreting exposure ages and erosion rates, *Earth and Planetary Science Letters*, 230, 163-175, 10.1016/j.epsl.2004.11.007, 2005.
- 445 Niedermann, S., Graf, T., Kim, J. S., Kohl, C. P., Marti, K., and Nishiizumi, K.: Cosmic-ray-produced ^{21}Ne in terrestrial quartz: the neon inventory of Sierra Nevada quartz separates, *Earth and Planetary Science Letters*, 125, 341-355, 10.1016/0012-821X(94)90225-9, 1994.



- 450 Nishiizumi, K., Klein, J., Middleton, R., and Craig, H.: Cosmogenic ^{10}Be , ^{26}Al , and ^3He in olivine from Maui lavas, *Earth and Planetary Science Letters*, 98, 263-266, [10.1016/0012-821x\(90\)90028-v](https://doi.org/10.1016/0012-821x(90)90028-v), 1990.
- Nishiizumi, K., Lal, D., Klein, J., Middleton, R., and Arnold, J. R.: Production of ^{10}Be and ^{26}Al by cosmic rays in terrestrial quartz in situ and implications for erosion rates, *Nature*, 319, 134-136, [10.1038/319134a0](https://doi.org/10.1038/319134a0), 1986.
- Nishiizumi, K., Imamura, M., Caffee, M. W., Southon, J. R., Finkel, R. C., and McAninch, J.: Absolute calibration of ^{10}Be
- 455 AMS standards, *Nuclear Instruments and Methods in Physics Research Section B: Beam Interactions with Materials and Atoms*, 258, 403-413, [10.1016/j.nimb.2007.01.297](https://doi.org/10.1016/j.nimb.2007.01.297), 2007.
- Spector, P. and Balco, G.: Exposure-age data from across Antarctica reveal mid-Miocene establishment of polar desert climate, *Geology*, 49, 91-95, [10.1130/g47783.1](https://doi.org/10.1130/g47783.1), 2020.
- Stone, J.: A Rapid Fusion Method for Separation of Beryllium-10 From Soils and Silicates, *Geochimica et Cosmochimica*
- 460 *Acta*, 62, 555-561, [10.1016/s0016-7037\(97\)00340-2](https://doi.org/10.1016/s0016-7037(97)00340-2), 1998.
- Stutz, J., Mackintosh, A., Norton, K., Whitmore, R., Baroni, C., Jamieson, S. S. R., Jones, R. S., Balco, G., Salvatore, M. C., Casale, S., Lee, J. I., Seong, Y. B., McKay, R., Vargo, L. J., Lowry, D., Spector, P., Christl, M., Ivy Ochs, S., Di Nicola, L., Iarossi, M., Stuart, F., and Woodruff, T.: Mid-Holocene thinning of David Glacier, Antarctica: chronology and controls, *The Cryosphere*, 15, 5447-5471, [10.5194/tc-15-5447-2021](https://doi.org/10.5194/tc-15-5447-2021), 2021.

465